

Characterization of Upper Indus Basin based on DEM Hypsometric Analysis

I. Ahmad^{1,3*}, Z. Ahmad^{1,2}, S. Munir³, Obaid-ur-Rehman³, S.R. Ali³ and Y. Shabbir³

¹Department of Earth Sciences, Quaid-e-Azam University, Islamabad, Pakistan

²ORIC, University of Wah, Wah Cantt, Pakistan

³Space Applications and Research Complex (SAR), SUPARCO, Islamabad, Pakistan

ARTICLE INFO

Article history :

Received : 15 May, 2017

Accepted : 12 April, 2018

Published : 13 April, 2018

Keywords:

Upper Indus Basin

Hypsometry

DEM

ABSTRACT

Assessment of geomorphic stages of catchment areas within Upper Indus Basin (UIB) is carried out through analysis of hypsometry. Hypsometric curves were extracted for each sub-basin from Digital Elevation Model (DEM) of Shuttle Radar Topography Mission (SRTM). Parameters of the Hypsometric Integral (HI), statistical moments like skewness, kurtosis, density skewness and density kurtosis of the curves were also analyzed. Study concluded that UIB is comprised of sub-basins of differential characteristics i.e., young, moderate and well developed. There is a correlation of 0.76 between the basin size and the HI. None of the basins appear to be in Monadnock Stage. The topographic analyses of slope, aspect and percentage snow-cover and land cover classes also validate the high erosion potential of upper reaches of Indus basin.

1. Introduction

Hypsometric analysis is mostly used to infer the temporal stages of geomorphic development and characterization of the basins/watersheds [1-7]. Tectonics, geology and climate interact to shape the morphology of the earth [8, 9]. Remote sensing data especially digital elevation model (DEM) is an effective source to extract the hypsometric profiles of an area. Hypsometric curves are important for land use development and planning and also for the management of natural hazards.

Hypsometry is the study of area with respect to different elevations. Hypsometric curve is a graph of relative area (a/A) versus relative height (h/H) whose shape represents the development history of the concerned basin [5]. Convex shaped curves represent younger less developed surfaces; concave shaped curves represent the oldest stage whereas S-shaped curves represent intermediate behavior or maturity stage. HI is an important parameter that signifies the stage of development of a basin and its characteristics as shown in Fig. 1. It is defined as the area under the hypsometric curve [5]. Higher the value of HI, the younger the surface is, however, different S-shaped curves may result in the same value for HI [4, 10].

Hypsometric curve representing the cumulative distribution of basin area with elevation succinctly captures the relief ratio and catchment volume [2, 5]. Several studies have used hypsometric analysis to characterize and differentiate different basins. For varying basin sizes, the spatial variation of HIs can serve as a first-step to assess factors that control landscape development [11]. It has been suggested that topography plays a significant role in determining the basin response [12, 13]. Hypsometry

inferred from different DEMs is shown to be stable against variations of resolution but still the drainage is found to affect the hypsometry hence suggesting scale dependence [10].

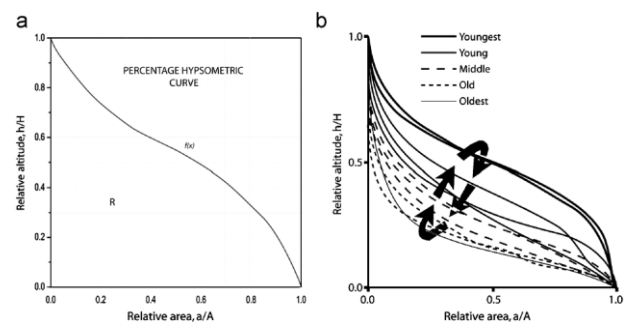


Fig. 1: (a) Hypsometric curve after Strahler [5], Area of region under curve (R) is known as HI, (b) Changes in hypsometric curves (modified from Ohmori [4]).

Some studies fail to show a correspondence between HI and indices of basin dimension, such as basin area and basin relief [11]. The HI value of 0.5 for a drainage basin seems critical in terms of landscape evolution. Equilibrium Line altitude is an important variable in determining the hypsometry of a glaciated basin [14]. Hypsometry of an individual basin may be greatly influenced by unique local conditions such as narrow outlets, major portion of hanging valleys or isolated geological structures [14].

1.1 Statistical Moments of Hypsometric Curves

According to the methodology developed by Harlin [15], if we treat the hypsometric curves as a cumulative probability distribution then we can compute the coefficients of skew and kurtosis for it. The technique consists of approximating the hypsometric curve by a

*Corresponding author : ijazbhutta@hotmail.com

continuous polynomial function. With relatively less undulations and inflexions of a hypsometric curve it can usually be approximated by a low order polynomial of 2nd or 3rd grade.

$$f(x) = a_0 + a_1(x_1) + a_2(x_2) + a_3(x_3) \dots + a_n(x_n) \quad (1)$$

The relative altitudes are represented by $f(x)$ whereas the relative areas are shown by x values. The coefficients $a_0, a_1, a_2 \dots a_n$ can be calculated through regression of the curve. The statistical moments of a hypsometric curve are often used to signify some interesting differentiating characters of a hypsometric curve and can thus be used to quantify changes in morphology of drainage basins. In basins with similar values of HI but different shapes these parameters become very important. The statistical moments used for description are given hypsometric skewness, hypsometric kurtosis, density skewness, density kurtosis. Skewness and Kurtosis describe the shape of a probability distribution compared to a normal distribution. Skewness and Kurtosis are the third and fourth moments about the x -mean as shown below by μ_3 and μ_4 respectively.

$$\mu_3 = \frac{1}{A} \int (x - \mu'_{01})^3 f(x) dx \quad (2)$$

$$\mu_4 = \frac{1}{A} \int (x - \mu'_{01})^4 f(x) dx \quad (3)$$

However, they are in the same units as variable- x and can be problematic in terms of scale so their coefficients called the hypsometric skew and hypsometric kurtosis are used as given below.

$$\text{Hypsometric Skew} = \frac{\mu_3}{\sigma_3} \quad (4)$$

$$\text{Hypsometric Kurtosis} = \frac{\mu_4}{\sigma_4} \quad (5)$$

Moreover, in a similar manner, density skewness and density kurtosis can be computed for the density function $g(x)$, where $g(x)$ is the derivative of $f(x)$,

Hypsometric skew and hypsometric kurtosis are related to erosion with hypsometric skew showing headwords erosion in upper reach whereas hypsometric kurtosis depicting erosion on both upper and lower portions of basin. Density skew and density kurtosis are related to slope with density skew denoting slope change and density kurtosis as mid-basin slope [15, 16].

The advancements in the field of GIS and availability of the satellite based DEMs have made hypsometric analysis even easier. The DEM resolution is not very significant to an appreciable degree [8, 10].

More eroded basins (concave) have a less total runoff as compared to a relatively less eroded (convex) basin. The dominant process in concave basin is through subsurface processes whereas in convex the surface response is higher. Hypsometric differences are also observed in the relations between base flow discharge and the mean groundwater depth and the variable source area. The flood response of a

basin is also closely related to hypsometric curve parameters [12]. Differences in hypsometric curves often reflect changes in erosion rates of a basin [17].

2. Study Area

UIB is situated in Northern Pakistan from latitude $23^\circ 42'$ to $37^\circ 05'$ N and longitude $66^\circ 09'$ to $81^\circ 49'$ E in the Hindukush - Himalayan (HKH) region, with a mean catchment elevation of 4400 m. The HKH region receives an annual precipitation ranging from 200 - 500 mm at lower altitudes and 1000 - 3000 mm at higher altitudes. The Indus river basin is divided into two portions with the catchment area above Tarbela Dam as the Upper Indus and below it as Lower Indus. UIB further consists of Gilgit, Hunza, Astor, Shyok, Shigar, Shingo, Zanskar sub-basins as shown in the Fig. 2.

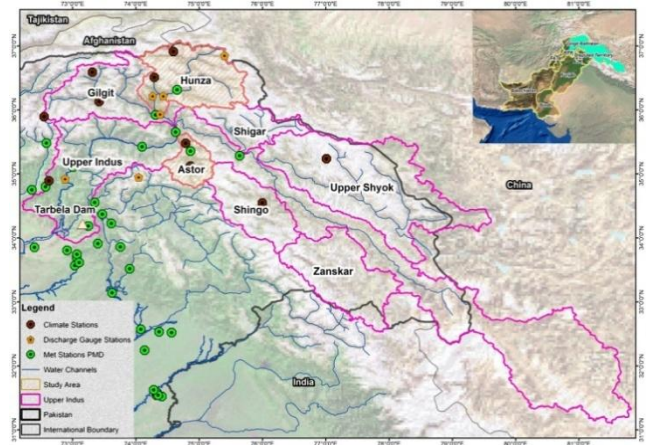


Fig. 2: Map of the study area.

There are 14 high altitude climate stations, 9 low altitude stations and 11 hydrological stations in UIB of Pakistan and a total of 11 discharge stations measuring the flow rates. Most of the stations are concentrated on the Northern side of UIB.

2.1 Geo-Tectonics of UIB

UIB is on the Eurasian side of the Indian European plate's collision. The geological age of UIB varies from Precambrian (1.8 billion years) to Cretaceous (100 million years). Most portions of the basins are older than 350 million years and only few regions are young.

The continent-continent collision between the Indian plate and Eurasian plate is responsible for the development of Himalayan mountain ranges. While the South Western side of the country has the triple plate junction where three tectonic plates, Indian plate, Eurasian plate and Ormorian plate are colliding together. The Chaman and Ornach-Nal fault system joins the North western Himalayan tectonic system to south western triple plate junction system. Due to such a unique tectonic location, Pakistan as a whole has experienced devastating earthquakes. The historic data shows that there was a significant increase of seismicity in

terms of frequency as well as intensity between 1897 and 1952 when 14 major earthquakes struck Pakistan. Nine of them were of magnitude > 7 ($M>7$) and five were of Magnitude > 8 ($M>8$). Among the tectonic system of Pakistan, the NW Himalayan Fold-and-Thrust Belt is considered as seismically one of the most active intercontinental regions of the world. Pakistan has suffered from many earthquake disasters in the past out of which October 2005 earthquake of Magnitude 7.6 and Quetta Earthquake in 1936 of Magnitude 8.2 were the most disastrous [18-20].

In the north Indian plate collided with the Eurasian plate and as a result formed an active fold-and-thrust belt on the northwestern margin of the Indo-Pakistan plate. This fold-and-thrust belt can be divided into two parts: the NW Himalayan belt and the Suleiman belt. The NW Himalayan belt is present along the transpressional zone while the Suleiman belt is present in the zone of Himalayan convergence [21]. Later on due to the collision of Indian plate with Eurasian plate there was an anticlockwise rotation which resulted in the transpressional zone which is 800-900 km long and Chaman and Ornach Nal fault was developed which is believed to be responsible for the transpression and it also delimits the western boundary of Indian plate [19]. In the main zone of convergence; some major thrusts were developed which are the Main Karakoram Thrust (MKT) also known as Shyok Suture, the Main Mantle Thrust (MMT) also called the Indus Suture, the Main Boundary Thrust (MBT) and the Salt Range Thrust (SRT). These thrusts subdivide the whole collision zone [18]. Here the area between MMT and SRT, including its westwards extensions i.e. Surghar, Marwat, Bhittani and Manzai ranges) are considered to be the part of NW-Himalayan Fold-and-Thrust Belt [19]. The southern boundary of these ranges are marked by thrusts. The Hazara Kashmir Syntaxis and the Nanga Parbat Harmosh Massif marks the eastern boundary of the belt. The western boundary is still not clearly explained but the Kurram fault in the south west and series of thrusts beyond the border of Pakistan are supposed to delineate the boundary.

NW Himalayan fold-and-thrust belt is almost 250 km wide and 560 km long and the Panjal-Khairabad fault divides it into the northern hinterland zone and southern foreland zone. The hinterland zone is also called Hazara Crystalline zone [18] and Himalayan Crystalline zone [19]. This hinterland zone is present between MMT and Panjal-Khairabad fault. It is composed of igneous and metamorphic rocks of Proterozoic to Mesozoic age. It exhibits a complex deformation pattern due to shearing and imbrications and basement is also involved in the process of thrusting. Six nappe zones i.e. Mohmand-Swat Nappe, Besham Nappe, Hazara Nappe, Banna Nappe, Kaghan Nappe and Nanga Parbat-Harmosh massif, are present in the hinterland and are separated by shears and thrust faults. The lower part of the hinterland zone in the south of

Mansehra thrust is composed of meta-sediments of Precambrian age. This part of the hinterland zone is also called the Khyber-Lower Hazara Meta-sedimentary Fold-and-thrust belt [18]. This meta-sedimentary belt is subdivided as Peshawar basin which is formed in Middle tertiary due to south verging imbricate thrusting on MBT. Peshawar basin has unlithified Quaternary sediments which indicates that deformation in this basin has involved both folding and faulting.

3. Material and Methods

Hypsometric curves are derived from DEMs. There are a range of freely available DEM data sources. The release of ASTER (Advanced Space-borne Thermal Emission and Reflection Radiometer) and SRTM (Shuttle Radar Topographic Mission) data has contributed significantly to the improvement of freely available DEM. Aster Global DEM has a resolution of nearly 30 m (1-arc-second) with an overall accuracy of around 17 m at the 95% confidence level, evaluated by the ASTER GDEM validation team [22].

One of the most widely used and validated source of DEM is Shuttle Radar Topography Mission data flown on Space Shuttle Missions by National Aeronautics and Space Administration (NASA) in 2000 to obtain elevation data for most of the world. The near-global coverage at a fairly high resolution of 1-arc second and being a publicly available dataset makes SRTM data highly suitable for current study. The SRTM version 4.1 from the USGS/NASA SRTM data covers up to 60 °N to 56 °S of the earth land surfaces. This version of the DEM was selected for extraction of hypsometric curves as this has been validated and refined by sophisticated interpolation and void filling algorithms which make use of ancillary data sources where they are available [23]. The accuracy of SRTM has been thoroughly tested by various studies and has been shown to be within range of ± 16 m [23- 26].

DEM data of SRTM having spatial resolution of 30 m was downloaded from site (<http://srtm.csi.cgiar.org>) [27]. It is available as 1-arc second Global elevation data in the form of $1^\circ \times 1^\circ$ tiles. It was in the form of regularly spaced grid of elevation points in Geo-referenced Tagged Image File Format (GeoTIFF) which is a TIFF file with embedded geographic information. The SRTM DEM specifications are mentioned in Table 1.

The geological data used in the study is from Geological Survey of Pakistan, 1964 [28]. The location individual climate and discharge stations were used from Water and Power Development Authority (WAPDA) and Pakistan Meteorology Department. The land cover data was used from Glob Land 30, a 30-m resolution Global Land cover dataset by National Geomatics Center of China.

Table 1: SRTM DEM characteristics sensor and product characteristics.

Satellite	Sensor	Capture Resolution	Pixel Resolution
Space Shuttle Endeavor	C-Band and X-Band	1 arc-second	30 meter
		3 arc-second	90 meter
		30 arc-second	1000 meter
Scene Type	Scene Size	Projection	
degree	1 degree latitude	Geographic	
	1 degree longitude		
WRS – 2	185 Kilometer	UTM	
	185 Kilometer		
Mosaic	Global	geographic	

3.1 Methodology

The downloaded individual tiles of SRTM DEM were mosaicked together to create a seamless raster of elevation values for the whole UIB as shown in Fig. 3. As a preprocessing step, the sinks were filled to create a filled DEM using Arc GIS 10.3 generic tool. The flow direction raster was calculated for the entire UIB using D8 algorithm. The D8 algorithm calculates possible flow directions at each cell towards the 8 neighboring cells [27, 28]. Flow accumulation was calculated for each cell depicting the number of cells from which water flows into a particular cell. The least cost algorithm is used to connect the stream flow directions in order to generate a continuous network of streams. All streams were vectorized and are assigned with a unique Strahler order, and the desired watersheds are extracted. The stream network is extracted from the flow accumulation and flow direction rasters for different Strahler orders automatically, e.g., 1, 2, 3 and so on [5].

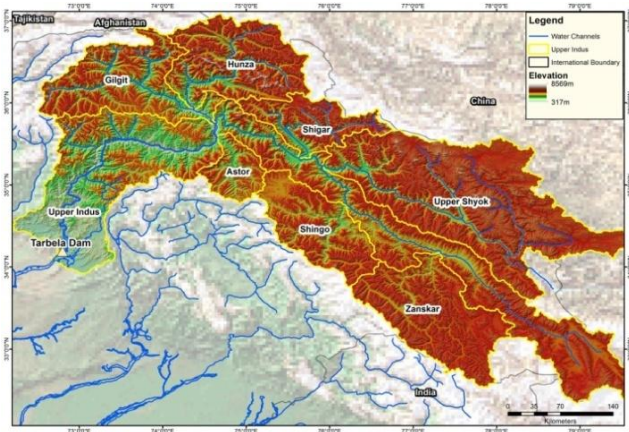


Fig. 3: Shaded relief of UIB from SRTM DEM.

The basins were seeded by analyzing the SRTM DEM to determine drainage points (cell). These points can also be referred to as the lowest point in the drainage basin.

For the purpose of extraction of hypsometric curves, an ArcGIS utility named CalHypso was used. Extension CalHypso in ArcGIS can be used to automatically extract

multiple hypsometric curves from DEM and calculate the main statistics related to the hypsometric curve by applying polynomial fits [29]. This extension was used to derive the hypsometric curves from the DEM and the statistical moments of these curves. DEM of UIB and the extents of sub-basins of UIB, namely Hunza, Astor, Shyok, Shigar, Gilgit, Shingo, Zanskar were used for this purpose. The remaining unnamed portion of UIB was labelled “Remaining Upper Indus Basin”. The HI values of each sub-basin were then joined to their respective area shapes and a map showing geographic distribution of the HI integrals was created. The statistical moments of hypsometric skewness, hypsometric kurtosis, density skewness and density kurtosis were then analyzed for their patterns. For the purpose of comparison, HI for each sub-basin was also calculated using the following formula:

$$H.I = \frac{(H_{mean} - H_{min})}{(H_{max} - H_{min})} \quad (6)$$

Where H denotes the respective elevations.

The geological ages were compared with the HIs and the correlation between basin size and HIs was established. Detailed extraction of the curve for Hunza, Astor and Upper Shyok basins was carried out using the attribute values of the DEM and then finding cumulative area, cumulative fraction of total area and fraction of max elevation. These values were used to find the mean of cumulative area and its corresponding elevation which was actually the mean hypsometric elevation. It is the elevation from which 50% of the area of a basin is above and the remaining 50% is below it. Each sub-basin was then divided into 500 m elevation zones as a precursor for use in Snowmelt Runoff Model (SRM). The process of extraction of hypsometric mean was repeated for each 500 m elevation zones. Slope and Aspect derived from DEM, along with Landcover of UIB were analyzed to qualitatively assess the erosion potentials among different sub-basins.

4. Results and Discussions

Based on the above mentioned adopted procedures, following results are obtained.

Hypsometric curves derived for each sub-basin are shown in Fig. 4. The lowest HI value of 0.376 is of Shigar basin and the Shingo basin has a value of 0.397. The highest HI value of 0.514 is of Zanskar basin followed by the second highest of 0.507 for Shyok basins. The remaining sub-basins lie in the range of 0.4-0.5 HI.

It is apparent that Shigar and Shingo are the oldest of the basins having an HI of 0.38 and 0.39 respectively. The youngest among these are Zanskar and Shyok basins with 0.51 HIs.

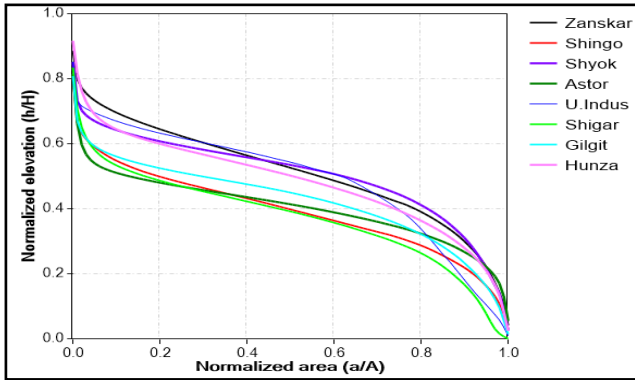


Fig. 4: Hypsometric curves of the sub-basins.

The mean HIs are also displayed in Fig. 5 with HI of Hunza and Gilgit basins between the youngest and oldest values. They also have moderate curves as shown in Fig. 4.

The spatial distribution of HI values of different sub-basins shows a pattern where the portions towards the South East are of higher HIs and the smaller central sub-basins of Astor, Shigar and Shingo have the lowest HI values. The North West sub-basins of Gilgit and Hunza have intermediate character as shown in Fig. 6.

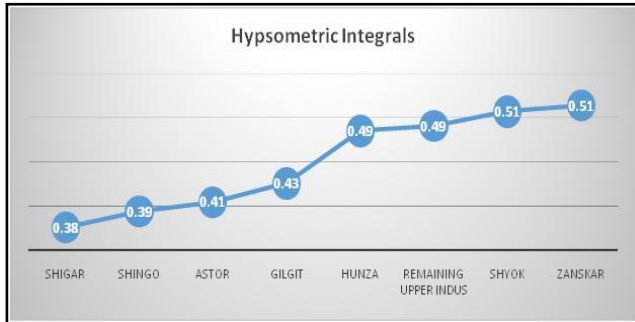


Fig. 5: Hypsometric curves of the sub-basins.

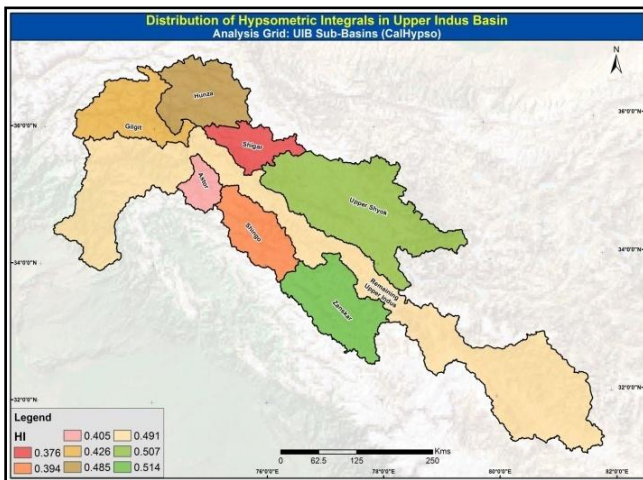


Fig. 6: Spatial distribution of HIs using Calhypso.

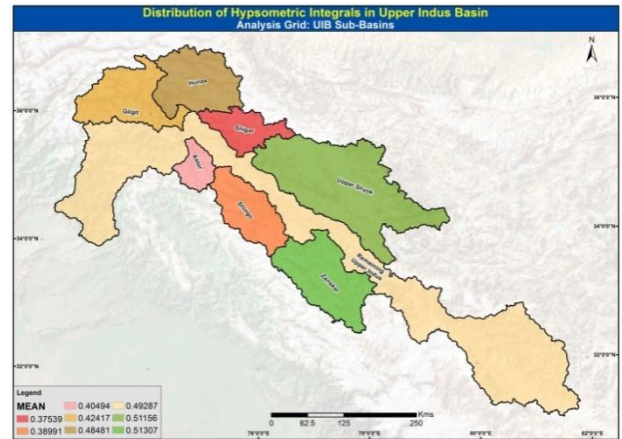


Fig. 7: Spatial distribution of HIs using (eq. 6).

The HI values derived through the use of (Eq. 6) are also shown spatially in Fig. 7. They correspond up to one-hundredth place with the values of HIs obtained through polynomial approximation using CalHypso, thus validating the results obtained through CalHypso.

The area denoted as remaining Upper Indus portion in Fig. 6 and Fig. 7 seem too wide and gross generalization of a larger area, if we split this area into two, we get the following curves (U.I. 1 and U.I. 2) as shown in Fig. 8. Fig. 8 shows that the westward side is significantly different from the eastward side with very different HI values i.e. the HI value for curve 2 is 0.327 suggesting that this portion is much older than curve 1 with 0.6 HI value.

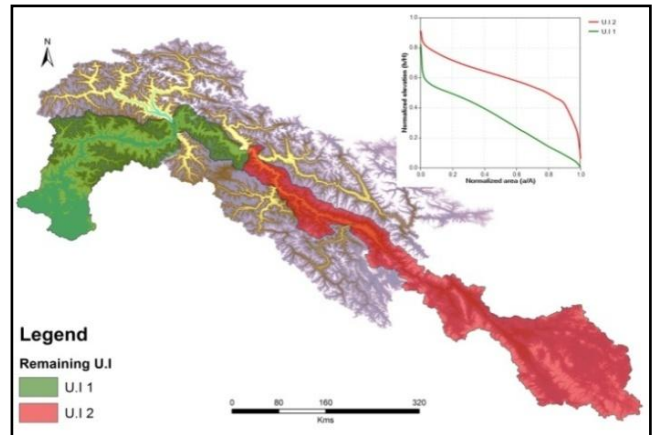


Fig. 8: Sub-portions of the remaining UIB.

When comparing the spatial distribution of HIs with the geological time-periods and the Fault maps (Fig. 9 and Fig. 10), it appears that the geological time-period of formation of Zanskar is much younger than the other basins which is also indicated by its highest HI value.

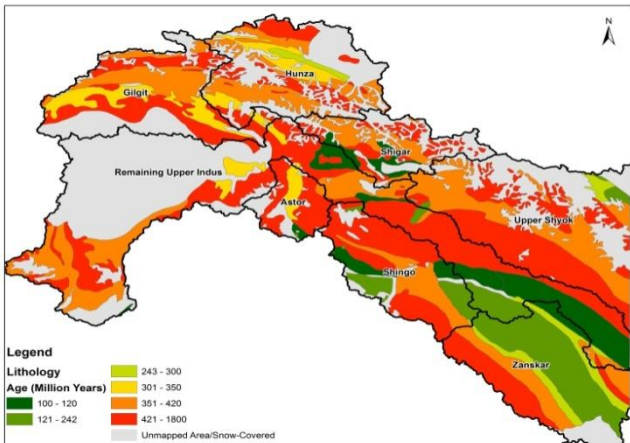


Fig. 9: Available geological ages of study area (Geological Survey of Pakistan, 1964) [28].

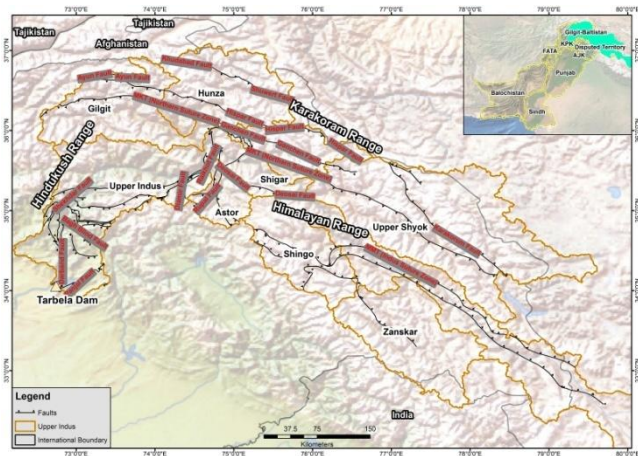


Fig. 10: Fault map (Geological Survey of Pakistan).

Many studies have discussed the dependence or independence of basin size or relief on hypsometric curve and integral [10, 11]. The correspondence between HI and indices of basin dimension, such as basin area and basin relief is in regards to the developmental stage of the basin [11]. Based on this study, we found a correlation of 0.74 ($R^2=0.54$) between HI values and basin size indicating the dependence of HI on basin size for the area under analysis as shown in Fig. 11. It has been suggested that topography plays a significant role in determining the basin response [12, 13].

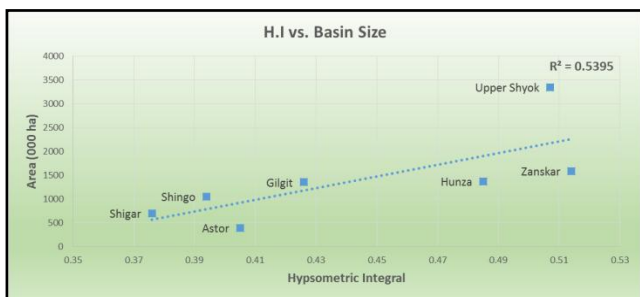


Fig. 11: Graph of H.I. vs. basin size.

The elevation of UIB ranges from 317 m near Tarbela and from the footsteps of Himalayas it rises to a maximum elevation of 8569 m. The portions above 7000 m mostly lie in Shigar and Hunza basins. The world's second highest peak K2 lies within UIB along with Gasherbrum, Broad Peak and Nanga Parbat, which is the Western most peak of Himalayan range, overlooking Indus River.

The range of elevation for Shigar basin is from 2185 m to 8569 m whereas for the Shyok basin the range is from 2289 m to 7803 m, even though their HIs are significantly different suggesting that elevation range cannot fully explain the difference in HIs.

HI alone is not an entirely descriptive feature of a surface, so we delve a little deeper using the statistical moments of the hypsometric curve. Skewness and kurtosis that describe probability distribution with respect to a normal distribution are compared. Hypsometric skew and hypsometric kurtosis is related to erosion. Skewness values suggest that Shigar and Shingo basins have highest headward erosion which is the erosion at the origin of a stream channel, causing the stream channel to lengthen while the erosion at both the upper and lower end of channel suggested by hypsometric kurtosis is not significantly different for each sub-basin. The highest value of hypsometric kurtosis is for Shigar and Shingo if we neglect the remaining UIB area.

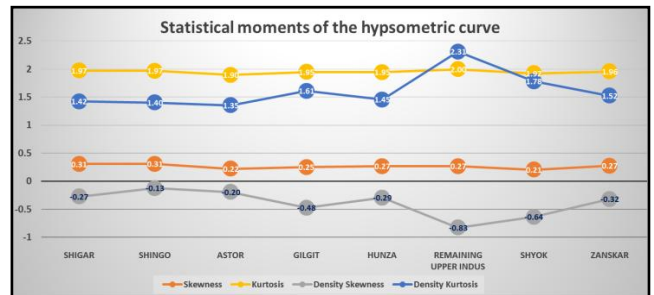


Fig. 12: Skewness, kurtosis, density skewness and density kurtosis UIB.

These statistical parameters become important in basins with similar values of HI but different shapes. Zaskar and Shyok basins, which have similar values of HI have different values of the statistical parameters. Zaskar, with a density kurtosis less than Shyok and a greater density skewness appears to have a more rigorous slope change than Shyok. The density skewness values are negative for all basins and is highest for Shingo basin and then for Astar basin signifying that for these basins slope change is maximum. Shyok and Gilgit basin have higher values of density kurtosis which signifies mid-basin slope (Fig. 12).

To explore in more detail the topographic character of Hunza, Astar and Shyok basins the three basins were divided into zones of 500 m elevation as a precursor for using them in Snowmelt Run-off Modeling. The percentage area for each 500 m elevation zone is shown in Fig. 13.

Table 2: Hypsometric mean elevations of zones.

	Zone	Area (Sq.Km)	Hypsometric Mean Elevation (m)	Zone	Area (Sq.Km)	Hypsometric Mean Elevation (m)	Zone	Area (Sq.Km)	Hypsometric Mean Elevation (m)		
Astor Basin	1	8.9	1554.5	Hunza Basin	1	106.1	Shyok Basin	1	243.4	2511	
	2	35.6	2028.5		2	236.7		2193	2	760.6	3073
	3	139.0	2526		3	509.4		2684.5	3	1236.3	3466
	4	342.5	2992		4	930.4		3182.5	4	2007.3	3986
	5	690.8	3492		5	1486.4		3678	5	3619.2	4490
	6	1146.8	3975.5		6	2252.7		4176	6	7708.5	5001.5
	7	1203.4	4419.5		7	3134.8		4667	7	12171.1	5439.5
	8	340.8	4835		8	3200.5		5133.3	8	5132.3	5858
	9	58.9	5377.5		9	1348.1		5566	9	500.0	6313.5
	10	21.4	5883		10	340.2		6089.5	10	61.5	6862.5
	11	8.1	6388		11	147.2		6595.4	11	6.4	7294
	12	2.9	6879.5		12	38.0		7045	12	0.0	7719.5
	13	1.5	7420		13	3.6		7480.5			
		14	0.1		7726						
	Total	3989	4061	Total	13733	4632	Total	33446.0	5251		

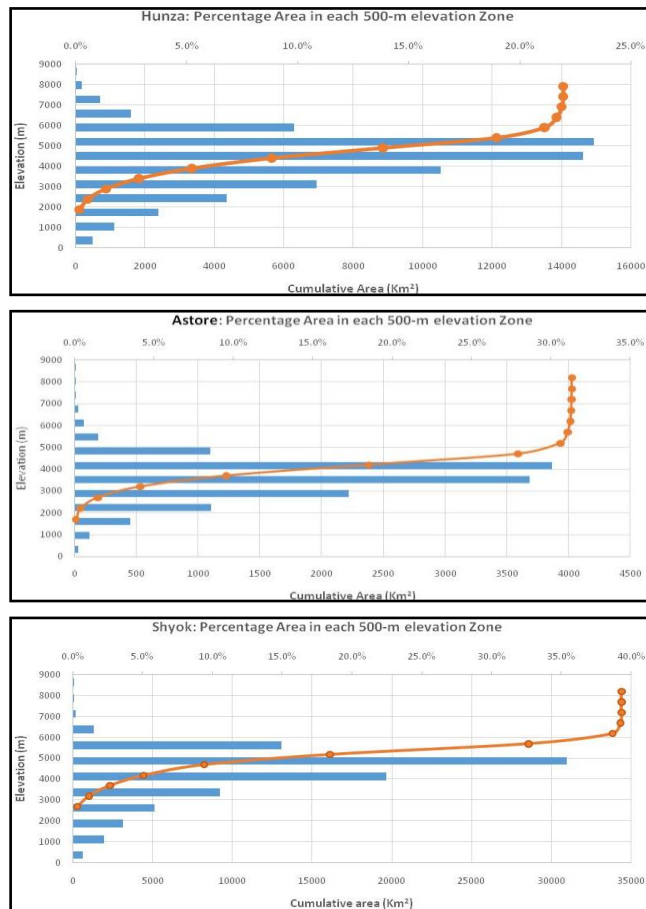


Fig. 13: Hypsometric curves of basin and distribution of area in 500-m elevation band.

It is evident from the graphs shown in Fig. 13 that the major portion of the basins lay in the intermediate elevation ranges with minor areal coverage in very high or low elevation zones. The most prominent such effect is in Shyok where very little areal coverage is in highest zones. Hunza has the most coverage in 4000-6000 m and a lot more percentage area in higher elevations than Astor and Shyok. This has profound implications on climate and snow fall/run-off. Hypsometric curve for the Hunza basin shows that elevation range of most of its area is from 3000 to 6000 m above mean sea level (a.m.s.l.). This accounts for more than 89 percent of total Hunza basin. Basin cumulative area above 5000 m elevation represents the mostly glaciated areas covering around 32 percent of the basin. Rest of basin area below 3000 m represents the least snow cover zones.

The slope and aspect derived for the entire UIB region is shown in Fig. 14. There is a large fluctuation in range of slopes within UIB with the top northern region having steeper slope ranges. In terms of landcover, Zanskar sub-basin is mostly bareland and Astor, Shingo, Gilgit sub-basins comprise of major grassland areas. Hunza, Shigar and Upper Shyok are dominated by snow/Ice. The steeper slopes on the shaded aspects having very less forested area becomes a recipe for higher erosion potential and thus act as active ground for recent neo-tectonics.

5. Conclusions

Based on the HIs, an assessment of time series of stages of geomorphic growth is determined highlighting sub-basins of differential character in UIB.

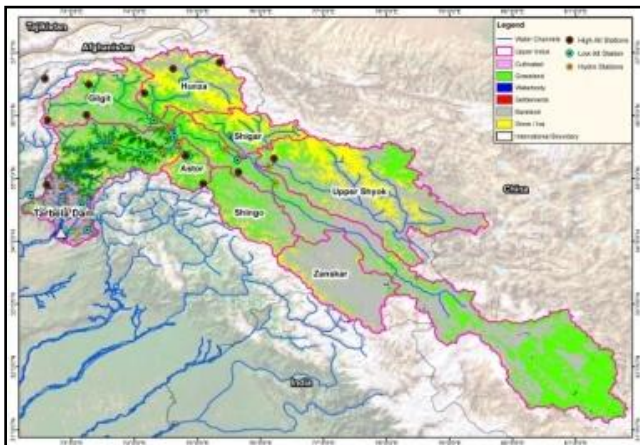
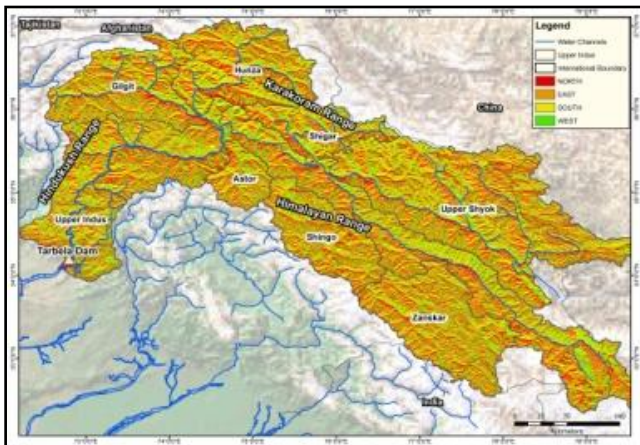
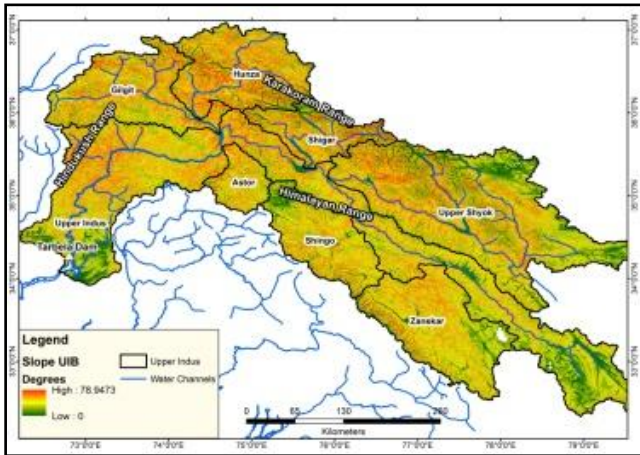


Fig. 14: Slope, aspect and landcover information of UIB.

The analysis suggests that the basins are of variable characters from young to well-developed through moderate showing that the area is sensitive to the recent tectonics. Shigar and Shingo basins being the oldest in terms of HI also have highest headword erosion. Zaskar and Shyok being the two youngest sub-basins, Zaskar appears to have a more rigorous slope change than Shyok. The size of the sub-basin in UIB plays a role in the speed of development

of the basin. Larger basins tend to be more developed than younger ones in UIB.

The analysis of neotectonics, however, requires a multi-faceted approach, based on integration of datasets from seismology, stratigraphy, geological structures, geodesy and satellite acquired information. These studies are important in management and evaluation of modifications in landcover and associated natural disasters.

Acknowledgement

The authors extend their thanks to the Water and Power Development Authority (WAPDA) NSIDC, USGS, SUPARCO and PMD for providing the required data. The authors would also like to thank Rana Ahmad Faraz and Muhammad Kamran for data collection and preliminary data evaluation.

References

- [1] Y.C. Chen, "Along-strike variations of morphotectonic features in the Western Foothills of Taiwan: tectonic implications based on stream-gradient and hypsometric analysis", *Geomorphology*, vol. 56, no. 1, pp. 109-137, 2003.
- [2] W.B. Langbein, "Topographic characteristics of drainage basins", Water-Supply Paper 968-C, US Government Printing Office, Washington, 1947.
- [3] N.A. Lifton, "Tectonic, climatic and lithologic influences on landscape fractal dimension and hypsometry: implications for landscape evolution in the San Gabriel Mountains, California", *Geomorphology*, vol. 5, no. 1-2, pp. 77-114, 1992.
- [4] H. Ohmori, "Changes in the hypsometric curve through mountain building resulting from concurrent tectonics and denudation", *Geomorphology*, vol. 8, no. 4, pp. 263-277, 1993.
- [5] A.N. Strahler, "Hypsometric (area-altitude) analysis of erosional topography", *Geological Society of America Bulletin*, vol. 63, no. 11, pp. 1117-1142, 1952.
- [6] G. Willgoose and G. Hancock, "Revisiting the hypsometric curve as an indicator of form and process in transport-limited catchment", *Earth Surface Processes and Landforms*, vol. 23, no. 7, pp. 611-623, 1998.
- [7] G. Willgoose, "A physical explanation for an observed area, slope and elevation relationship for catchments with declining relief", *Water Resources Research*, vol. 30, no. 2, pp. 151-159, 1994.
- [8] A. Azor, E.A. Keller and R.S. Yeats, "Geomorphic indicators of active fold growth: South Mountain–Oak Ridge anticline, Ventura basin", *Geo-science World*, vol. 114, no. 6, pp. 745-753, 2002.
- [9] S.A. Mahmood, "Analyzing spatial autocorrelation for the hypsometric integral to discriminate neotectonics and lithologies using DEMs and GIS", *GIS and Remote Sensing*, vol. 48, no. 4, pp. 541-565, 2011.
- [10] J.E. Hurtrez, "Effect of drainage area on hypsometry from an analysis of small scale drainage basins in the Siwalik Hills (Central Nepal)", *Earth Surface Processes and Landforms*, vol. 24, no. 9, pp. 799-808, 1999.
- [11] R.C. Walcott and M.A. Summerfield, "Scale dependence of hypsometric integrals: An analysis of southeast African basins", *Geomorphology*, vol. 96, no. 1-2, pp. 174-186, 2008.
- [12] A.D. Howard, "Role of hypsometry and platform in basin hydrologic response", *Hydrological Processes*, vol. 4, no. 4, pp. 373-385, 1990.
- [13] M.E. Marani, "Geomorphic controls on regional base flow", *Water Resources Research*, vol. 37, no. 10, pp. 2619-2630, 2001.
- [14] S.H. Brocklehurst, "Hypsometry of glaciated landscapes", *Earth Surface Processes and Landforms*, vol. 29, no. 7, pp. 907-926, 2004.

- [15] J.M. Harlin, "Statistical moments of the hypsometric curve and its density function", *Mathematical Geosciences*, vol. 10, pp. 59–72, 1978.
- [16] W.A. Luo, "A theoretical travel time based on watershed hypsometry", *Journal of the American Water Resources Association*, vol. 39, pp. 785–792, 2003.
- [17] J.G. Masek, B.L. Isacks, T.L. Gubbels and E.J. Fieldings, "Erosion and tectonics at the margins of continental plateaus", *Journal of Geophysical Research*, vol. 99, no. B7, pp. 13941-13956, 1994.
- [18] R.A.K. Tahirkheli, M. Mattauer, F. Proust and P. Tapponier, "The India-Eurasia suture zone in northern Pakistan: Some new data for interpretation at plate scale, in *Geodynamics of Pakistan*", Geological Survey Pakistan, Eds: A. Farah, and K.A. DeJong, pp. 125–130, 1979.
- [19] M. Lisa, A.A. Khwaja and M.Q. Jan, "Seismic Hazard Assessment of the NW Himalayan Fold-and-Thrust Belt, Pakistan, Using Probabilistic Approach", *J. Earthquake Engineering*, vol 11, no. 2, pp. 257-301, 2007.
- [20] I.A.K. Jadoon, "Thin-skinned tectonics on continent/ocean transitional crust, Sulaiman Range, Pakistan", Ph.D. thesis. Geology Dept. Oregon State University, USA, 1992. Retrieved from <https://ir.library.oregonstate.edu/downloads/vt150m664>
- [21] A.H. Kazmi and M. Jan, "Geology and Tectonics of Pakistan", Graphic Publishers, 5-C, 6/10 Nazimabad Karachi, Pakistan, ISBN 969-8375-00-7, pp. 819-842, 1997.
- [22] Advanced Spaceborne Thermal Emission and Reflection Radiometer (ASTER), *Global Digital Elevation Model (GDEM), Version 2*, 2011.
- [23] A. Koch and P. Lohmann, "Quality assessment and validation of digital surface models derived from the Shuttle Radar Topography Mission (SRTM)", *International Archives of Photogrammetry and Remote Sensing*, vol. XXXIII, Supplement B4. Amsterdam, 2000.
- [24] C.M. George, and C. Paraschou, "Vertical accuracy of the SRTM DTED level 1 of Crete", *International Journal of Applied Earth Observation and Geoinformation*, vol. 7, pp. 49-59, 2005, doi:10.1016/j.jag.2004.12.001.
- [25] SRTM 90m Digital Elevation Database v4.1. <http://www.cgiar-csi.org/data/srtm-90m-digital-elevation-database-v4-1>, as accessed on 30th of September, 2013.
- [26] J.P. Muller, "Quantitative assessment of C-band and X-band SRTM datasets over the CEOS-WGCVTMSG test sites and inter-comparison of C-band and DEM with the OS, PANORAMA DTM", 2005.
- [27] A. Jarvis, H.I. Reuter, A. Nelson and E. Guevara., "Hole-filled SRTM for the globe Version 4", available from the CGIAR-CSI SRTM 90 m database (<http://srtm.csi.cgiar.org>), 2008.
- [28] M.A. Bakr, R.O. Jackson, *Geological map of Pakistan*, Geological Survey of Pakistan, 1964.
- [29] J.V. Pérez-Peña, J.M. Azañón, A. Azor, "CalHypso: An ArcGIS extension to calculate hypsometric curves and their statistical moments. Applications to drainage basin analysis in SE Spain", *Computers & Geosciences*, vol. 35, no. 6, pp 1214-1223, 2009.